Nonreactive molecular dynamics force field for crystalline hexahydro-1,3,5-trinitro-1,3,5 triazine

Sylke Boyd[a] and Matthew Gravelle
Division of Science and Mathematics, University of Minnesota, Morris, Morris, Minnesota 56267

Peter Politzer
Department of Chemistry, University of New Orleans, New Orleans, Louisiana 70148

(Received 12 December 2005; accepted 17 January 2006)

An empirical nonreactive force field has been developed for molecular dynamics (MD)/Monte Carlo simulation of the formation, diffusion, and agglomeration of point defects in the crystal lattice of the α modification of hexahydro-1,3,5-trinitro-1,3,5 triazine (RDX) using flexible molecules. Bond stretching and angle bending are represented by Morse and harmonic functions, and torsion by a truncated cosine series. Nonbonded interactions, both inter- and intramolecular, are described by Buckingham potentials separately parametrized. Intermolecular electrostatic interactions are treated via a Coulomb term coupled with a smooth 15.0 Å cutoff radius. Parameters were taken in part from earlier published works and were determined partly by fitting to known molecular and crystal properties of RDX. In MD simulations at constant pressure and temperature, the model was able to stabilize and maintain the correct crystal structure, symmetry, and molecular conformation of α-RDX. Vibrational frequencies, lattice binding energy and dimensions, coefficients of thermal expansion, and several unusually short intermolecular distances are all reproduced in satisfactory agreement with experimental data. © *2006 American Institute of Physics*.
[DOI: 10.1063/1.2176621]

I. INTRODUCTION

In recent years, one of the primary objectives in the field of energetic materials has been to reduce sensitivity, by which is meant vulnerability to detonation or violent deflagration caused by accidental external stimuli. The latter can include impact, shock, friction, heat, etc. The challenge is to find an optimum balance between a high level of energetic performance and a low sensitivity.

In general, several factors—including molecular composition and structure, crystal properties, and physical state—are involved in determining the sensitivity of a compound. There have been numerous attempts to relate it solely to molecular features, such as stoichiometry, the strengths of key bonds ("trigger linkages"), and electrostatic potentials. Some of these correlations, which are reviewed elsewhere,[1,2] are quite successful, perhaps surprisingly so, although they are usually limited to a particular chemical class of compounds. It is clear, however, that a comprehensive approach to diminishing sensitivity requires that crystal effects be taken into account.

It is widely believed that a key role in the initiation of detonation is played by "hot spots."[3–11] These are small regions in the crystal in which is localized thermal energy produced by the conversion of the mechanical energy of, for example, impact or shock. If sufficient thermal energy is channeled into appropriate vibrational modes, it can lead to bond rupture and begin chemical decomposition. The initial steps are endothermic, but they are followed by exothermic processes which release energy and thus sustain and expand the decomposition. The first observation of an early exothermic step, the formation of H_2O, was reported by Sharma *et al.* in a study of 1,3,5-triamino-2,4,6-trinitrobenzene (TATB).[5]

Hot spots have been characterized in terms of dimensions, temperatures, and durations by Tarver *et al.*[12] Their formation is commonly attributed to the presence of lattice defects, such as vacancies, interstitial occupancies, misalignments, edge, and screw dislocations, etc.[7,9,10,13–19] By one interpretation, the externally introduced energy relieves the strain in the lattice due to the defect by allowing relaxation or rearrangement. This results in a localization of energy in the neighborhood of the defect, giving rise to a hot spot.[9,13,14] An example would be the collapse of a vacancy due to a passing shock wave.[18–20] Several molecular dynamics (MD) simulations have shown the development of hot spots in conjunction with lattice defects.[9,10,14,17] (It should be noted that Dlott and co-workers have argued that hot spots can form even in the absence of defects, provided that there is an efficient means of transferring energy into particular anharmonic vibrational modes.[7,21])

In view of the generally acknowledged significance of lattice defects in relation to detonation initiation, it would be highly desirable to have an enhanced understanding of how their generation can be controlled and modified. Accordingly we wish to develop a molecular dynamics/Monte Carlo methodology for simulating the natural formation of point defects under growth conditions in the crystal lattices of energetic solids. It would then be possible to investigate how

[a]Author to whom correspondence should be addressed. Electronic mail: sboyd@morris.umn.edu

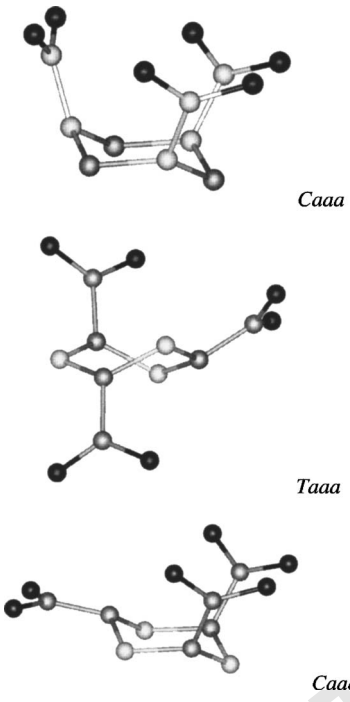

FIG. 1. Three conformers of the RDX molecule. Hydrogens are not shown.

this is affected by temperature and pressure. The first step, the results of which are reported in this paper, has been to develop an appropriate inter-/intramolecular force field. It should stabilize the correct molecular and crystal structures of the compound and satisfactorily reproduce its properties, including molecular conformations and relative orientations without sacrificing the flexibility of the molecules. This must be achieved for relatively large molecules having many conformational options. The point defects of interest will involve a considerable amount of lattice disruption around their sites, and only a model with both inter- and intramolecular degrees of freedom will be able to provide the necessary insight into the defects' structural and dynamic properties.

II. PROCEDURE

A. System

We chose to focus initially upon the prominent secondary explosive hexahydro-1,3,5-trinitro-1,3,5-triazine, 1 (RDX). The molecule has numerous possible conformations, since the ring can be chair (C), boat (B), or twist (T), and th e nitro groups axial (a) or equa torial (e). The RDX molecule is *Caae* with a C_S symmetry in the solid;[22,23] in the gas phase, on the other hand, the situation is more ambiguous. Electron diffraction[24] and *ab initio* calculations[25–27] indicate *Caaa*, C_{3v}, although with several low-lying conformers separated by less than 1.2 kcal/mol.[25,26] However, there have also been arguments favoring a dynamical interconversion between them.[23,28] Three conformers of the RDX molecule, including the *Caae* and *Caaa*, are shown in Fig. 1.

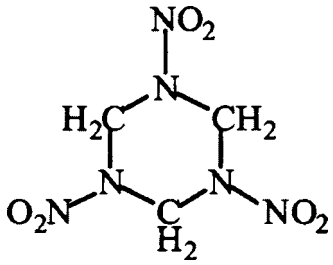

There are two crystalline polymorphs labeled (1) α and β, the former predominating under normal conditions.[22,23] Crystalline α-RDX has a *Pbca* symmetry with an orthorhombic unit cell containing eight molecules,[22,23] which are in interlocked pairs.[29]

B. Model

Our simulation cell contained $3\times3\times3$ unit cells, each having eight molecules, for a total of 4536 atoms. Periodic boundary conditions were imposed in all directions. While lattice angles were constrained at 90°, the lattice parameters have been allowed to vary in constant-pressure MD simulations. The treatment of long-range electrostatic interactions included a smooth cutoff function. We found a range of 15.0 Å to be an optimal compromise between the requirements to avoid an overlap, to include centers on next-nearest neighbors, and to be computationally efficient.

Constant-pressure, constant-temperature molecular dynamics (NPT-MD) was performed using an Andersen/Berendsen algorithm for pressure and temperature control.[30] The time step varied between 0.2 and 0.8 fs, depending upon the temperature and the expected velocities. All of the simulations were performed at a pressure of 1 atm. Geometry optimizations were via a conjugate-gradient minimization with respect to the particle positions, with convergence criteria of 0.05 kcal/Å mol for the large models and 0.0001 kcal/Å mol for single molecules. Vibrational properties were obtained from the eigenmodes of the Hessian matrix. All simulations were run on either an XP2000 Compaq workstation or a Beowulf cluster of 16 Xeon processors.

We identified the ring conformation of the RDX molecule during a simulation by means of the normalized box product of the ring diagonals, which is close to zero for boat and twist conformers but about ±0.5 for the complementary chair forms. The orientations of the nitro groups, axial or equatorial, were assessed by projecting the N–N bonds onto the axis normal to the average plane of the ring (the ring normal vector); from this could be determined the angles of the NO_2 groups relative to this axis.

C. Force field

1. Background

A number of intra- and/or intermolecular force fields have been proposed for energetic nitro compounds. Wallis and Thompson constructed a potential energy surface for the RDX molecule[31] which was subsequently refined and extended in scope.[32–34] Sorescu *et al.* developed a viable intermolecular force field for RDX within the rigid molecule approximation.[35] This describes well the equilibrium crystal

TABLE I. Parameters for the angle bending, torsion, and nonbonded terms in the intramolecular potential.

Angle bending

Angle	θ° (degree)	k (kcal/mol rad^2)
C–N–C	115.000 000	145.000 000
C–N–N	116.300 000	130.000 000
N–C–N	109.400 000	145.334 935
N–C–H	110.571 577	58.274 924
N–N–O	117.250 000	125.000 000
O–N–O	125.500 000	205.484 711
H–C–H	105.100 000	56.180 756

Torsion[a]

Atoms i,j,k,l	a_1^{ijkl}	b_1^{ijkl}	a_2^{ijkl}	b_2^{ijkl}	a_3^{ijkl}	b_3^{ijkl}
C, N, N, O	2.00	2	−0.5740	4	0	0
C, N, C, N	3.30	1	−1.61	2	0.110	3
C, N, C, H	−0.16	3	0	1	0	1

Intramolecular nonbonded

Atoms i,i[b]	A_{ii} (kcal/mol)	B_{ii} (Å^{-1})	C_{ii} (Å^6 kcal/mol)
C, C	65 380.3	3.686	227.26
N, N	135 119.0	4.132	236.4
O, O	4 358.7	4.545	4.305
H, H	47 945.6	4.630	42.417
O, H[c]	174 348.0	6.73	16.40

[a]The units for a_1^{ijkl}, a_2^{ijkl}, and a_3^{ijkl} are kcal/mol.
[b]The formulas for treating mixed pairs of atoms are given in the text.
[c]Separate parameters are assigned for O···H hydrogen bonds.

properties of RDX as well as a series of other nitro compounds.[36] Smith and Bharadwaj established a force field for octahydro-1,3,5,7-tetranitro-1,3,5,7-tetrazocine[37] (HMX), a molecule that is structurally very similar to RDX. However, our tests of different combinations of these earlier potentials did not find any that stabilized the α-RDX crystal lattice with flexible molecules in the correct conformation.

A very promising force field has emerged recently, the ReaxFF,[38–40] which consists basically of a partial bond order potential. It has been used to examine the progression of shock waves in a computer model of crystalline RDX.[40] This force field is good for investigating reactive processes because no assumptions concerning reaction pathways need to be made. However the lengthy simulations of large systems that will be required in this work make computational speed essential. Traditional empirical force fields can handle such nonreactive processes very efficiently.

2. Present force field: Intramolecular

Our intramolecular potential consisted of four terms:

$$U_{\text{intra}} = U_{\text{bond}} + U_{\text{bend}} + U_{\text{torsion}} + U_{\text{intrananonbonded}}. \quad (1)$$

Bond stretching U_{bond} was represented by a Morse function, which will permit bond breaking, with the parametrization of Wallis and Thompson.[31] Angle bending U_{bend} was treated harmonically; the force constants and equilibrium angles, listed in Table I, were modified from those of Chambers and Thompson[32] to yield the vibrational frequencies of the NO_2 scissor and certain ring modes.

Following the others,[32,37] we expressed the torsional potential as a truncated cosine series:

$$U_{\text{torsion}} = \sum_{\text{torsions}} \sum_{m=1}^{3} a_m^{ijkl}(1 - \cos b_m^{ijkl}\varphi_{ijkl}). \quad (2)$$

In Eq. (2), φ_{ijkl} is the dihedral angle between the atoms i, j, k, and l. The parameters of Chambers and Thompson[32] did not stabilize the *Caae* conformer. However, those suggested by Smith and Bharadwaj[37] for HMX proved to be a good starting point for RDX as well. We changed their C,N,N,O values to adjust the $N-NO_2$ rotational barrier to 4.0 kcal/mol, which is intermediate between what is in the literature[32,37] and the result of a B3PW91/6-31G* calculation.[41] The torsional parametrization is in Table I.

Nonbonded intramolecular interactions between atoms separated by more than three bonds, $U_{\text{intrananonbonded}}$, were treated by means of a Buckingham potential.[42] We wrote the Buckingham potential in terms of the parameters of the Lennard-Jones 6-12 potential,[43] ε and r^0, since they have clear physical interpretations; thus,

$$U_{\text{intrananonbonded}} = \frac{1}{2}\sum_i \sum_j \varepsilon_{ij}\left[\frac{6}{a_{ij}-6}\exp\left\{-a_{ij}\left(\frac{r_{ij}}{r_{ij}^0}-1\right)\right\} - \frac{a_{ij}}{a_{ij}-6}\left(\frac{r_{ij}^0}{r_{ij}}\right)^6\right], \quad (3)$$

in which r_{ij} is the distance between atoms i and j. The steepness parameter α_{ij} would be roughly 15 for the Lennard-Jones potential. The force field was parametrized in terms of ε, r^0, and a. The normal Buckingham form of the potential

$$U_{\text{intranonbonded}} = \frac{1}{2}\sum_i \sum_j A_{ij}\exp(-B_{ij}r_{ij}) - \frac{C_{ij}}{r_{ij}^6} \quad (4)$$

was used throughout all simulations; the parameters A, B, and C are related to the Lennard-Jones parameters as

$$A_{ij} = \frac{6\varepsilon_{ij}}{a_{ij}-6}\exp(a_{ij}) \quad B_{ij} = \frac{a_{ij}}{r_{ij}^0}, \quad C_{ij} = \frac{\varepsilon_{ij}a_{ij}}{a_{ij}-6}(r_{ij}^0)^6. \quad (5)$$

The parameters A_{ii}, B_{ii}, and C_{ii}, given in Table I, are based on those of Wallis and Thompson for a Lennard-Jones 6-12 potential.[31] For mixed pairs of atom types, the values were obtained by the formulas $A_{ij}=\sqrt{A_{ii}A_{jj}}$, $B_{ij}=\frac{1}{2}(B_{ii}+B_{jj})$, and $C_{ij}=\sqrt{C_{ii}C_{jj}}$. Separate parameters were assigned for O···H hydrogen bonds. This was necessary since their nature is not simply following from mixing the O···O or H···H interactions.

Initially, we considered a "wag" term to govern the movements of the NO_2 groups relative to the C–N–C plane. The two stable out-of-plane positions of the NO_2 are responsible for the axial and equatorial orientation.[44] We found that the correct orientations were sufficiently reproduced by the intramolecular nonbonded interactions and omitted such a term from the intramolecular energy.[5]

3. Intermolecular

The intermolecular potential U_{inter} is generally written as a sum of electrostatic and nonbonded contributions:

$$U_{\text{inter}} = U_{\text{electrostatic}} + U_{\text{internonbonded}}. \quad (6)$$

Several such force fields have been proposed in earlier studies of energetic materials[32,35,37] and used successfully in their contexts. For our system of flexible RDX molecules, however, they led to distorted lattice dimensions and incorrect molecular conformations. Accordingly, we have developed a new intermolecular potential, albeit with the form of Eq. (6).

The electrostatic term $U_{\text{elctrostatic}}$ was expressed via a Coulomb expression, coupled with a cutoff function f_c:

$$U_{\text{electrostatic}} = \sum_M \sum_N \sum_{i\supset M} \sum_{j\supset N} f_c(r_{ij})\frac{1}{4\pi\varepsilon_0}\frac{q_i q_j}{r_{ij}}. \quad (7)$$

The quantities q_i and q_j are the net charges on atoms i in molecule M and j in N; ε_0 is the permittivity of vacuum. The function $f_c(r_{ij})$ is defined by

$$f_c(r_{ij}) = \begin{cases} 1 \text{ for } r_{ij} < r_o \\ 1 - 10\left(\dfrac{r_{ij}-r_o}{r_c-r_o}\right)^3 + 15\left(\dfrac{r_{ij}-r_o}{r_c-r_o}\right)^4 - 6\left(\dfrac{r_{ij}-r_o}{r_c-r_o}\right)^5 \text{ for } 4.0 \leqslant r_{ij} \leqslant r_c \\ 0 \text{ for } r_{ij} > r_c \end{cases} \quad (8)$$

The onset radius r_o was chosen at 4 Å, while the cutoff distance r_c of 15.0 Å allows us to include next-nearest-neighbor interactions but yet keep the size of the system computationally feasible. For intermolecular nonbonded interactions $U_{\text{internonbonded}}$ we again used a Buckingham potential, as in Eqs. (3)–(5), with a different parametrization. These long-range interactions decay somewhat faster than the Coulomb interactions, where the cutoff distances are larger than 15 Å.

Including the atomic charges, our complete intermolecular potential U_{inter} required that 20 parameters be determined by fitting to known crystal properties. The set of 20 will be designated by $\{\chi_k\}$, where $k=1,2,\ldots,20$. The fitting was accomplished by means of a function $\Phi(\{\chi_k\})$ that was designed to minimize the differences between certain computed and experimental properties of α-RDX in constant-pressure molecular dynamics simulations:

$$\Phi(\{\chi_k\}) = \varphi_{\text{energy}} + \varphi_{\text{lattice}} + \varphi_{\text{morientations}} + \varphi_{\text{separations}} + \left(\sum_i q_i\right)^2. \quad (9)$$

The first term, $\varphi_{\text{energy}}=E(\{\chi_k\}) - \Delta H_{\text{sub}}$, compares the binding energy of the current optimized crystal structure to the known enthalpy of sublimation of α-RDX. Minimizing $\varphi_{\text{lattice}}=\Sigma_{i=1}^3[L_i(\{\chi_k\})-L_i^0]^2$ should give good approximations to the correct lattice dimensions L_i^0. The term $\varphi_{\text{orientations}} = -\langle[\mathbf{n}^0\cdot\mathbf{n}(\{\chi_k\})]^2\rangle$ compares the ring normal vectors of the molecules in an optimized structure with the ones of the ideal crystal. $\varphi_{\text{separations}}=\langle(r_{ij}(\{\chi_k\})/r_{ij}^0)^2 - 2(r_{ij}(\{\chi_k\})/r_{ij}^0)\rangle$ is intended to account for several unusually short intermolecular distances that are present in α-RDX;[22] r_{ij} is the distance between the atoms involved. Finally, the last term ensures that the total charge is close to zero.

The minimization of $\Phi(\{\chi_k\})$ was achieved with a basic Monte Carlo algorithm and simulated annealing to adjust the $\{\chi_k\}$ toward the minimum energy configuration. After each change in the parameters, the crystal structure was optimized with respect to its total energy. This ensured that φ_{energy} used a near-equilibrium value within the current force field and also allowed the structural terms in $\Phi(\{\chi_k\})$ to exert their effects. The Monte Carlo procedure produced a selection of "islands" of optimum $\{\chi_k\}$ for $\Phi(\{\chi_k\})$. These islands were restricted further by reoptimizing $\Phi(\{\chi_k\})$, using a conjugate-gradient routine. This rather extended procedure yielded the parameter set in Table II. It is important to understand that these parameters represent a compromise between the various requirements we defined for our fitting function. While no particular fitting criterion is met exactly, we still were

TABLE II. Parameters for intermolecular potential.

Electrostatic			
Atom i	q_i (electron units)		
C	0.057 52		
N	−0.137 20		
N (nitro)	0.271 57		
O	−0.267 24		
H	0.100 81		
Intermolecular nonbonded			
Atoms i,i[a]	A_{ii} (kcal/mol)	B_{ii} (Å^{-1})	C_{ii} (Å^6 kcal/mol)
C, C	597 281.49	3.126 49	6198.56
N, N	1 080 539.06	4.525 47	1088.55
O, O	6 964 643.00	6.256 84	343.21
H, H	433 245.35	4.702 57	368.89
O, H[b]	3 627 521.50	7.153 62	53.187

[a]The formulas for treating mixed pairs of atoms are given in the text.
[b]Separate parameters are assigned for O···H hydrogen bonds.

able to find a parameter set that very well represents the system in the given basis of potential energy functions.

The molecular dynamics and force field code can be obtained from the authors. The images of structures in the figures were produced by the freely available visualization package GOPENMOL.[46,47]

III. RESULTS AND DISCUSSION

A. Molecular properties

The intramolecular force field stabilized chair and twist conformers, but not boat, which were unstable and rearranged into twist. Table III lists the computed geometries for the *Caaa*, *Caae*, and *Taaa* forms. Our *Caaa* bond lengths and angles are in overall good agreement with Rice and Chabalowski's B3LYP/6-311+G** results,[26] the largest difference being for the N–N distances. The C–N–N–O torsional

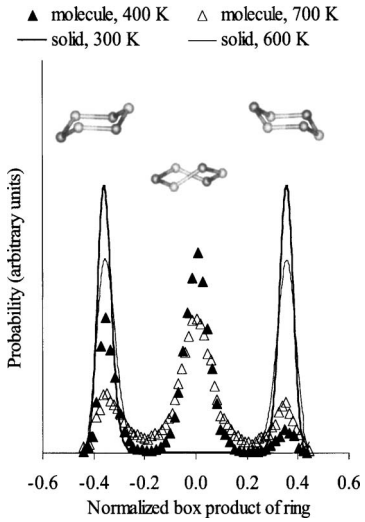

FIG. 2. Probabilities of chair and twist/boat conformers in NPT-MD simulations.

angles, ±17.4°, are close to the ±19° of Shishkov *et al.*[24] Our *Caae* values are nearly all within the range observed by neutron diffraction[22] for crystalline α-RDX.

The ground state of the isolated molecule was found to be *Caaa* but only 0.014 kcal/mol lower in energy than the *Caae* (the stable conformer in the crystal[22,23]) and 1.55 kcal/mol below the *Taaa*. This is consistent with the general conclusion that there are several low-lying interconverting conformers in the gas phase, with very similar energies,[23,25,26,28] reflecting the flexible nature of the molecules.

Figures 2–5 show the effect of crystalline environment upon conformer stability. The data represent ensemble averages resulting from MD simulations over 2 ns for the isolated molecule and 200 ps at a pressure of 1 atm for the solid.

TABLE III. Geometries of RDX conformers.

	Caaa		*Caae*		*Taaa*
Bond lengths (Å)					
	Present work B3LYP/6-311+G**[a]		Present work[b]	α-RDX, experimental[c]	Present work[b]
C–N	1.455	1.4607	1.455	1.440–1.468	1.455
N–N	1.380	1.4234	1.380	1.351–1.398	1.380
N–O	1.210	1.2156	1.210	1.201–1.233	1.210
C–H	1.081	1.0886	1.081	1.058–1.092	1.081
Angles (degree)					
	Present work B3LYP/6-311+G**[a]		Present work[b]	α-RDX, experimental[c]	Present work[b]
C–N–C	115.5	115.73	115.2	114.6–115.1	115.5
N–C–N	109.5	112.45	109.3	107.8–111.7	109.9
C–N–N	116.7	118.01	116.3	115.6–120.9	116.6
N–N–O	117.2		117.1	116.8–117.8	117.1
O–N–O	125.5	126.98	125.4	125.0–125.7	125.4
Dihedral angles (degree)					
	Present work		Present work[b]		Present work[b]
C–N–C–N	+51.7, −51.8		+52.4, −52.4		+59.4, −28.6
C–N–N–O	+17.4, −17.4		+16.3, −16.3		+16.4, −15.2

[a]Reference 26. Average values are listed.
[b]The angles are average values.
[c]Reference 22.

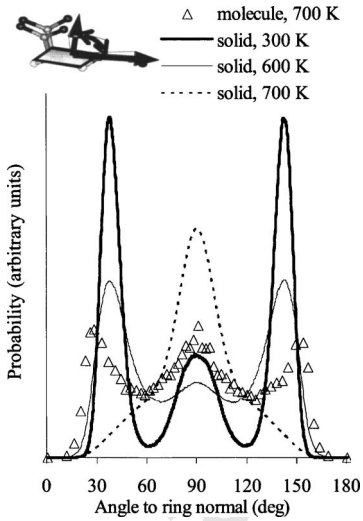

FIG. 3. Probabilities of axial and equatorial orientations of NO_2 groups. Angles of 40° and 140° to ring normal correspond to the axial; 90° indicates the equatorial.

Figure 2 indicates the probabilities of ring conformers, these having been identified by the normalized box product of the ring diagonals (Sec. II B). At 400 K, the isolated molecule is frozen into one of the chair conformations, whereas at 700 K, the twist is most likely, arguably as an intermediate in rearranging from one chair to an other. The crystal stabilizes the chair conformations; there is no indication of any twist or boat.

A second relevant feature of the RDX molecule is the orientation of the NO_2 groups with respect to the ring normal vector (the axis perpendicular to the average plane of the ring); 40° and 140° correspond to the axial, 90° to the equatorial. For the solid, which should be composed of *Caae* conformers, it can be seen in Fig. 3 that the axial orientations do indeed dominate at 300 and at 600 K. At 700 K, however, the equatorial has the highest probability in the solid, and for the isolated molecule it is roughly equal to the two axial states. It may be that the high temperature causes rapid transitions between the two axial states, decreasing their probabilities and increasing that of the intermediate equatorial.

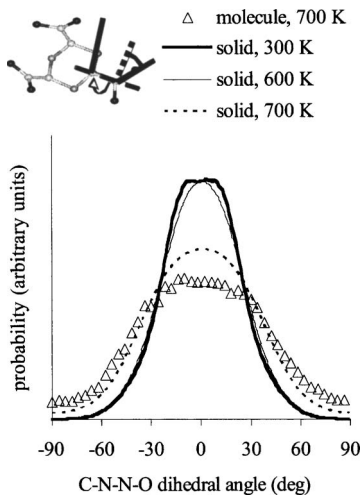

FIG. 4. Probabilities of NO_2 dihedral angles (torsional motion).

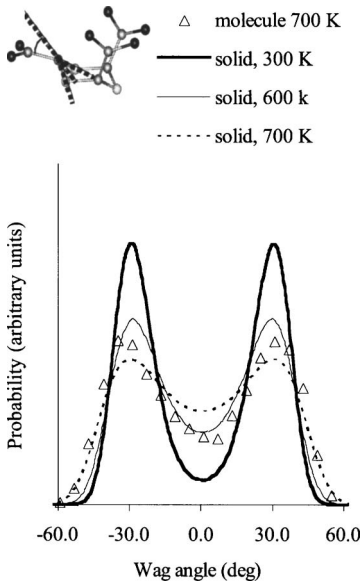

FIG. 5. Probabilities of wag angles of NO_2 groups with respect to C-N-C planes.

Two other types of motion that are examined are torsional around the N–N bonds and wagging of the NO_2 groups with respect to the C–N–C planes. The C–N–N–O dihedral angles are primarily in the vicinity of 0° (Fig. 4), although the spread is significantly greater in the isolated molecule and in the solid phase at 700 K. For the NO_2 wag, there are clearly two favored angles (Fig. 5), at ±30° out of the C–N–C planes; the barrier is less than 1 kcal/mol. Experimentally, Filhol *et al.* have found wag angles of 21.5°, 32.4°, and 33°.[48]

As one means of assessing the quality of our intramolecular force field, we calculated the vibrational frequencies of the isolated *Caae* conformer. These are compared in Table IV to those observed for α-RDX (Ref. 49) and to other computed values.[26,31] Our overall agreement with the experimental and other results is quite satisfactory. Of particular interest to us are the vibrational states between 200 and 700 cm^{-1}, which have been described as "doorway modes" for the transfer of energy from lattice phonons to the molecular vibrations involved in bond breaking.[50] The assignments of particular modes in the table corresponds to the results of our model; the references are arranged to match the frequency intervals.

B. Crystal properties

NPT molecular dynamics was carried out over 200 ps at 1 atm pressure and at various temperatures. The time step was 0.8 fs between 100 and 400 K, and 0.5 fs between 450 and 700 K. Table V presents the ground-state crystal properties derived from our optimized model. The corresponding experimental data are also included, as are those obtained by Sorescu *et al.* in MD simulations with a rigid molecular force field.[35]

The binding energy of our system, with respect to separation into individual molecules, was 27.7 kcal/mol. The measured enthalpy of the sublimation of RDX, which was used as one of our fitting criteria, is 31.1 kcal/mol.[51]An

TABLE IV. Calculated and experimental vibrational frequencies for the *Caae* conformer of RDX (in cm^{-1}). The infrared experimental data are for the α polymorph of the solid.

Present work				
Our assignment	Frequency	MD, single molecule[a]	B3LYP/ 6-311+G**[b]	Infrared[c]
NO_2 twist	28(2)	38(2)	44	
			60	
	32	41	63	
	39(2)	52(2)		
NO_2 wag	46	57	74	
	98		93	
	105		107	104
	137			
NO_2 wag and rock	177	178(2)		
			209	208
	221	249	229	223
	241	257		
	289	261(2)	290	
Ring	294	316(2)	325	300
	319	343		345
	381	424(2)	371	410
			403	
	401	438(2)	406	
NO_2 sway	475	441	438	461
	494	495	463	486
Ring	512		579	
	538			
NO_2 scissor	594	582	588	588
	603	648(2)	610	602
	690		651	670
CH_2 wag	708	741(2)	676	738
	713		756	
NO_2 scissor	758	776(2)	761	755
	765		769	
Ring	795	807	803	783
CH_2 rock and twist	847	877	855	844
			870	853
			896	883
	914		909	915
	933		937	926
	939	956	951	947
	998	1027(2)	1011	1019
	1015			
	1029	1038(2)	1036	1040
	1061			
		1052		
CH_2 scissor	1140	1165(2)	1153	1219
	1150		1230	1234
	1279	1185	1238	1271
	1282	1285	1264	1275
	1288	1290(2)	1270	1310
			1296	1320
			1299	1330
CN stretch	1376	1335(2)	1337	1352
			1362(2)	
	1377	1382		1377
			1374	1389
	1414		1406	1423
			1420	1434
		1466	1468	1459
			1480	
NN stretch	1548	1519(2)	1496	1532
	1566			1540
	1574	1554(3)		1573
NO stretch	1593		1623	1591
	1597		1648	1598
	1600		1668	
CH stretch	3001(2)	2982(3)	3015	2855
			3016	2922
	3002		3081	2948
	3056	3051(3)	3199	3001
	3057		3205	3066
	3060		3206	3075

[a]Reference 31.
[b]Reference 26.
[c]Reference 49.

agreement to within 11% on this parameter is reasonable and sufficient for our purpose and certainly compares with the performance of other methods with respect to the binding energy.[52]

As required, the system's ground state symmetry is *Pbca*, and all of the molecules are stable in the correct *Caae* conformation. Our lattice dimensions at 300 K differ from the observed by an average of 1.8% (Table V); the resulting density, 1.854 g/cm^3, is 2.7% higher than the experimental.[22,51,53] These results for the binding energy and lattice dimensions were verified with a larger simulation cell having $4\times4\times4$ unit cells and 512 molecules.

Below about 100 K, the model crystal is composed entirely of *Caae* conformers (Fig. 6). The proportion of *Caae* decreases with increasing temperature; this can be attributed primarily to the more rapid wagging motion of the equatorial NO_2, which produces *Caaa*.

In order to confirm that the molecular orientations are within the limits set by the requirement of the *Pbca* symmetry, we monitored the variations with temperature of the angles φ and θ between the ring normal vectors and the L_3 axis, with φ being measured within the L_1-L_2 plane. These occur in two combinations: $(\varphi,\theta)=(46°,102°)$ and $(-46°,78°)$. Figure 7 shows that these values were maintained to about 600 K, although there were increasingly large fluctuations already around 500 K.

The model disintegrated above 650 K; this was manifested in a sharp decrease in the density (Fig. 8), in sudden changes in conformer populations (Fig. 6) and molecular ori-

TABLE V. Calculated and experimental crystal properties of α-RDX.

Property	Present work	MD, rigid molecules[a]	Experimental
Binding energy (kcal/mol)	27.7		31.1[b] ($\Delta H_{\text{sublimation}}$)
Lattice dimensions at 300 K (Å)	12.998 11.278 10.857	13.396 11.798 10.732	13.182[c] 11.574 10.709
Density at 300 K (g/cm^3)	1.854	1.740	1.806[c]
Coefficients of linear thermal expansion (K^{-1})	35.4×10^{-6} 43.4×10^{-6} 77.5×10^{-6}	34.8×10^{-6} 47.5×10^{-6} 47.2×10^{-6}	63.6×10^{-6}[d]
Coefficient of volume thermal expansion (K^{-1})	158×10^{-6}	129.6×10^{-6}	191×10^{-6}[d]
Bulk modulus (GPa)	18		13.0[e]
Formation energy of vacancy (kcal/mol)	51.2		

[a]Reference 35.
[b]Reference 51.
[c]Reference 22.
[d]Reference 54.
[e]Reference 39.

entations (Fig. 7), and in the transition from an orthorhombic to a cubic cell. Since the melting point of α-RDX is known to be 204.1 °C (477.3 K),[51] it is evident that we are not satisfactorily simulating the solid→liquid transition, perhaps because our intermolecular force field was established entirely on the basis of crystal properties.

The variation in our lattice dimensions with temperature can be seen in Fig. 9. We found the coefficients of the linear thermal expansion

$$\alpha_i = \frac{1}{L_i}\left(\frac{\partial L_i}{\partial T}\right)_P \tag{10}$$

to differ for the three lattice dimensions, as did Sorescu *et al.*[35] Only one experimental value has been reported,[54] and our results compare well with the experiment as well as with Ref. 35. The coefficient of the volume thermal expansion

$$\beta = \frac{1}{V}\left(\frac{\partial V}{\partial T}\right)_P \tag{11}$$

has been derived from the variation of density with temperature (see Fig. 9). It is given in Table V.

Isotropic expansion and compression of the system with subsequent reoptimization yield a bulk modulus of 18 GPa. While this is higher than the experimental 13.0 GPa (Ref. 39) (Table V), we consider it to be quite satisfactory, given that this property was not among those fitted.

In Fig. 10 are the radial distribution functions for some intermolecular pairs of atoms at temperatures from 150 to 700 K. As was mentioned earlier, neutron diffraction has revealed several groups of unusually short intermolecular distances in α-RDX:[22] O···H, 2.46 Å; O···O, 2.94 Å; N···O, 2.99 Å, and N···N, 3.01 Å. It is notable that our model does reproduce most of these reasonably well.

Finally, we estimated the formation energy of a single vacancy by removing one RDX molecule from the original model, reoptimizing, and calculating ΔE for the process

Original system (216 molecules)→Final system (215 molecules)+RDX molecule. (12)

This gave 51.2 kcal/mol, which includes the binding energy of a single molecule plus the subsequent strain energy of the lattice. Our result falls between those from two density functional treatments, 39.1 and 78.3 kcal/mol.[55] The structural shifts in the immediate vicinity of the vacancy affect mostly the nitro side arms of the neighboring molecules and are in general miniscule.

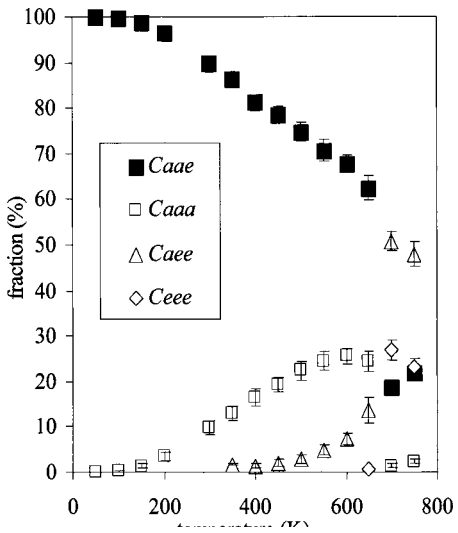

FIG. 6. Probabilities of chair conformers in crystal at various temperatures.

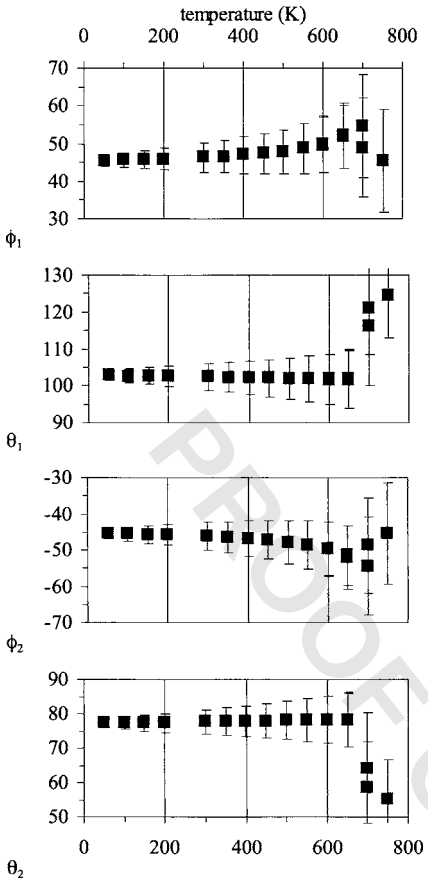

FIG. 7. Molecular orientations in crystal at various temperatures. φ and θ are the angles between the ring normal vectors and the L_3 axis, φ being measured within the L_1-L_2 plane.

IV. SUMMARY

A new empirical force field has been developed for the study of structural and

dynamical features of point defects in crystals composed of relatively large but flexible molecules. While the intermolecular potential was fitted specifically to the properties of α-RDX, the same approach can be applied to other energetic compounds. What is very significant is that the model does succeed in stabilizing the correct molecular conformer and

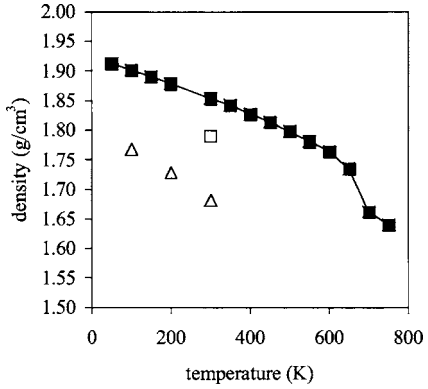

FIG. 8. Variation of crystal density with temperature. Solid squares show present results. Triangles indicate those of Sorescu *et al.* (Ref. 35) Empty squares correspond to the experimental density at 300 K (Ref. 22).

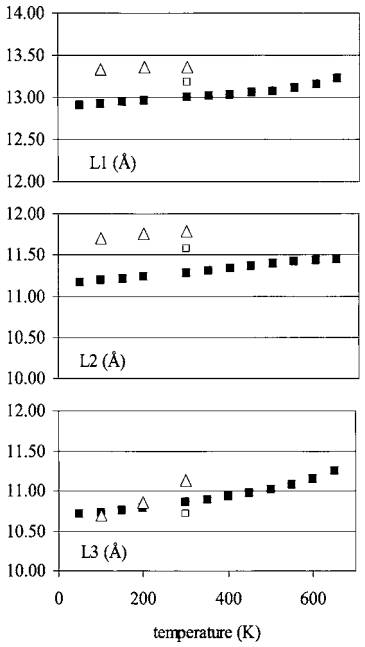

FIG. 9. Variation of lattice dimensions with temperature. Solid squares present our results triangles indicate those of Sorescu *et al.* (Ref. 35). Empty squares correspond to experimental values at 300 K (Ref. 22).

crystal structure of α-RDX, and in maintaining the stability and integrity of the system over an extended period of time and increases in temperature. Various molecular and lattice properties were reproduced in satisfactory agreement with experimental data. We are currently completing a work on the investigation of vacancies, divacancies, and orientational defects and will follow this paper with a publication of these results.

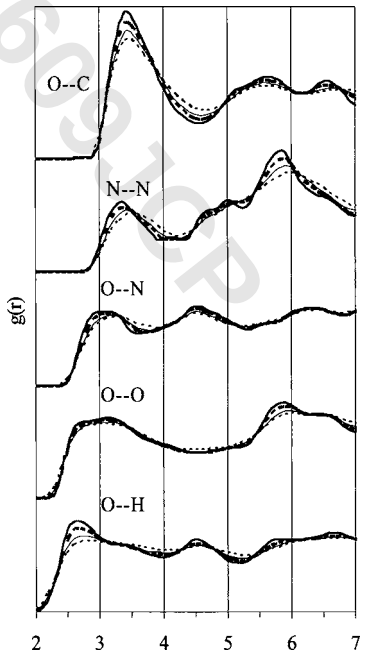

FIG. 10. Radial distribution functions for several intermolecular pairs of atoms in crystal, at different temperatures: thick solid curves, 150 K; thin solid curves, 300 K; dotted curves, 600 K; and dash-dot curves, 700 K.

ACKNOWLEDGMENTS

We greatly appreciate the support of the Office of Naval Research (Contract No. N00014-99-1-0393) and Project Officer Dr. Judah M. Goldwasser. We are also grateful to the University of Minnesota Grant-in-Aid program and its Undergraduate Research Opportunities Program. One of the authors (S.B.) wants to thank Kevin J. Boyd for many enlightening discussions.

[1] P. Politzer and H. E. Alper, in *Computational Chemistry: Reviews of Current Trends* edited by J. Leszczynski (World Scientific, Singapore, 1999), Vol. 4, chap. 6.
[2] P. Politzer and J. S. Murray, in *Energetic Materials. Part 2. Detonation, Combustion*, P. Politzer and J. S. Murray, eds. (Elsevier, Amsterdam, 2003), chap. 1.
[3] F. P. Bowden and A. D. Yoffe, *Fast Reactions in Solids* (Butterworths, London, 1958).
[4] M. J. Kamlet and H. G. Adolph, *Proceedings of the Seventh Symposium (International) on Detonation* (Naval Surface Warfare Center, Silver Springs, MD 1981) Report No. NSWCMP-82-334, p. 84.
[5] J. Sharma, J. C. Hoffsommer, D. J. Glover, C. S. Coffey, F. Santiago, A. Stolovy, and S. Yasuda, in *Shock Waves in Condensed Matter*, edited by J. R. Asay, R. A. Graham, and G. K. Straub (Elsevier, Amsterdam, 1984), p. 543.
[6] P. Maffre and M. Peyrard, Phys. Rev. B **45**, 9551 (1992).
[7] A. Tokmakoff, M. D. Fayer, and D. D. Dlott, J. Phys. Chem. **97**, 1901 (1993).
[8] L. E. Fried and A. J. Ruggiero, J. Phys. Chem. **98**, 9786 (1994).
[9] D. H. Tsai and R. W. Armstrong, J. Phys. Chem. **98**, 10997 (1994).
[10] J. W. Mintmire, D. H. Robertson, and C. T. White, Phys. Rev. B **49**, 14859 (1994).
[11] W. Holmes, R. S. Francis, and M. D. Fayer, J. Chem. Phys. **110**, 3576 (1999).
[12] C. M. Tarver, S. K. Chidester, and A. L. NicholsIII, J. Phys. Chem. **100**, 5794 (1996).
[13] R. W. Armstrong, C. S. Coffey, V. F. DeVost, and W. L. Elban, J. Appl. Phys. **68**, 979 (1990).
[14] D. H. Tsai, J. Chem. Phys. **95**, 7497 (1991).
[15] R. S. Sinkovits, L. Phillips, E. S. Oran, and J. P. Boris, Mater. Res. Soc. Symp. Proc. **296**, 161 (1993).
[16] J. Sharma, C. S. Coffey, A. L. Ramaswamy, and R. W. Armstrong, Mater. Res. Soc. Symp. Proc. **418**, 257 (1996).
[17] C. T. White, J. J. C. Barrett, J. W. Mintmire, M. L. Elert, and D. H. Robertson, Mater. Res. Soc. Symp. Proc. **418**, 277 (1996).
[18] M. M. Kuklja, Appl. Phys. Lett. A **76**, 359 (2003).
[19] A. P. Ershov, N. P. Satonkina, and G. M. Ivanov, Tech. Phys. Lett. **30**, 63 (2004).
[20] A. E. D. M. van der Heijden and R. H. B. Bouma, Cryst. Growth Des. **4**, 999 (2004).
[21] X. Hong, S. Chen, and D. D. Dlott, J. Phys. Chem. **99**, 9102 (1995).
[22] C. S. Choi and E. Prince, Acta Crystallogr., Sect. B: Struct. Crystallogr. Cryst. Chem. **B28**, 2857 (1972).
[23] R. J. Karpowicz and T. B. Brill, J. Phys. Chem. **88**, 348 (1984).
[24] I. F. Shishkov, L. V. Vilkov, M. Kolonists, and B. Rozsondai, Struct. Chem. **2**, 57 (1991).
[25] N. J. Harris and K. Lammertsma, J. Am. Chem. Soc. **119**, 6583 (1997).
[26] B. M. Rice and C. F. Chabalowski, J. Phys. Chem. A **101**, 8720 (1997).
[27] D. Chakraborty, R. P. Muller, S. Dasgupta, and W. A. GoddardIII, J. Phys. Chem. A **104**, 2261 (2000).
[28] T. Vladimiroff and B. M. Rice, J. Phys. Chem. A **106**, 10437 (2002).
[29] R. J. Karpowicz and T. B. Brill, J. Phys. Chem. **87**, 2109 (1983).
[30] H. J. C. Berendsen, J. P. M. Postma, W. F. van Gunsteren, A. DiNola, and J. R. Haak, J. Chem. Phys. **81**, 3684 (1984).
[31] E. P. Wallis and D. L. Thompson, J. Chem. Phys. **99**, 2661 (1993).
[32] C. C. Chambers and D. L. Thompson, J. Phys. Chem. **99**, 15881 (1995).
[33] P. M. Agrawal, D. C. Sorescu, B. M. Rice, and D. L. Thompson, Fluid Phase Equilib. **155**, 166 (1999).
[34] Y. Guo and D. L. Thompson, J. Phys. Chem. B **103**, 10599 (1999).
[35] D. C. Sorescu, B. M. Rice, and D. L. Thompson, J. Phys. Chem. B **101**, 798 (1997).
[36] D. C. Sorescu, B. M. Rice, and D. L. Thompson, J. Phys. Chem. A **103**, 989 (1999).
[37] G. D. Smith and R. K. Bharadwaj, J. Phys. Chem. B **103**, 3570 (1999).
[38] A. C. T. van Duin, S. Dasgupta, F. Lorant, and W. A. GoddardIII, J. Phys. Chem. A **105**, 9396 (2001).
[39] A. Strachan, A. C. T. van Duin, D. Chakraborty, S. Dasgupta, and W. A. GoddardIII, Phys. Rev. Lett. **91**, 98301 (2003).
[40] A. Strachan, A. C. T. van Duin, and W. A. GoddardIII, AIP Conf. Proc. **706**, 895 (2004).
[41] M. C. Concha (private communication).
[42] A. D. Buckingham, P. W. Fowler, and J. M. Hutton, Chem. Rev. (Washington, D.C.) **88**, 963 (1988).
[43] J. E. Lennard-Jones, Trans. Faraday Soc. **28**, 333 (1932).
[44] P. P. Ewald, Ann. Phys. **64**, 253 (1921).
[45] M. P. Allen and D. J. Tildesley, *Computer Simulations of Liquids* (Oxford Science, Oxford, 1987).
[46] L. Laaksonen, J. Mol. Graphics **10**, 33 (1992).
[47] D. L. Bergman, L. Laaksonen, and A. Laaksonen, J. Mol. Graphics Modell. **15**, 301 (1997).
[48] A. Filhol, C. Clement, M.-T. Forel, J. Paviot, M. Rey-Lafon, G. Richoux, C. Trinquecoste, and J. Cherville, J. Phys. Chem. **75**, 2056 (1971).
[49] M. Rey-Lafon, C. Trinquecoste, R. Cavagnat, and M.-T. Forel, J. Chim. Phys. Phys.-Chim. Biol. **68**, 1533 (1971).
[50] S. Ye, K. Tonokura, and M. Koshi, Combust. Flame **132**, 240 (2003).
[51] *LASL Explosive Property Data*, edited by T. R. Gibbs and A. Popolato, (University of California Press, Berkeley, 1980).
[52] W. F. Perger, J. Zhao, M. Blanco, and R. Pandey, AIP Conf. Proc. **706**, 251 (2004).
[53] J. Köhler and R. Meyer, *Explosives*, 4th ed. (VCH, Weinheim, Germany, 1993).
[54] M. Dobratz, *Properties of Chemical Explosives and Explosive Simulants* (Lawrence Livermore National Laboratory, Livermore, CA, 1981), Report No. UCRL 52997 pp. 19-131–19-132.
[55] M. M. Kuklja and A. B. Kunz, J. Appl. Phys. **86**, 4428 (1999).